Expression Dynamics of NADPH Oxidases During Early Zebrafish Development

Cory J. Weaver,[1] Yuk Fai Leung,[1] and Daniel M. Suter[1,2]*

[1]Department of Biological Sciences, Purdue University, West Lafayette, Indiana 47907
[2]Bindley Bioscience Center, Purdue University, West Lafayette, Indiana 47907

ABSTRACT

Nicotinamide dinucleotide phosphate oxidases (NOX) control various cellular signaling cascades. In the nervous system, there is recent evidence that NOX-derived reactive oxygen species (ROS) regulate neurite outgrowth, regeneration, and stem cell proliferation; however, a comprehensive NOX gene expression analysis is missing for all major model systems. Zebrafish embryos provide an excellent model system to study neurodevelopment and regeneration because they develop quickly and are well suited for in vivo imaging and molecular approaches. Although the sequences of five NOX genes (*nox1, nox2/cybb, nox4, nox5*, and *duox*) have been identified in the zebrafish genome, nothing is known about their expression pattern. Here, we used quantitative polymerase chain reaction combined with in situ hybridization to develop a catalog of *nox1, nox2/cybb, nox5*, and *duox* expression in zebrafish during early nervous system development from 12 to 48 hours post fertilization. We found that expression levels of *nox1, nox5*, and *duox* are dynamic during the first 2 days of development, whereas *nox2/cybb* levels remain remarkably stable. By sectioning in situ hybridized embryos, we found a pattern of broad and overlapping NOX isoform expression at 1 and 1.5 days post fertilization. After 2 days of development, a few brain regions displayed increased NOX expression levels. Collectively, these results represent the first comprehensive analysis of NOX gene expression in the zebrafish and will provide a basis for future studies aimed at determining the functions of NOX enzymes in neurodevelopment and regeneration. J. Comp. Neurol. 524:2130–2141, 2016.

INDEXING TERMS: NADPH oxidase; expression, nervous system development; zebrafish (RRID:ZIRC_ZL1)

Reactive oxygen species (ROS) are a class of small molecules that can oxidize many biomolecules including proteins and lipids. Overproduction of ROS has been implicated in a number of diseases including hypertension, neurodegenerative conditions, and cancer (Montezano and Touyz, 2014; Nakanishi et al., 2014; Nayernia et al., 2014). However, when produced in a controlled fashion in response to a specific stimulus, ROS also act as critical signaling intermediates in a growing number of cellular signaling pathways regulating multiple biological processes including cell differentiation, migration, and death (Finkel, 2011; Forman et al., 2014). Although there are several sources of ROS within the cell, one class of enzymes called nicotinamide dinucleotide phosphate (NADPH) oxidases (commonly abbreviated NOX) are especially interesting in the context of cellular signaling, because these enzymes can be activated and inactivated by a variety of mechanisms, including by cytosolic proteins and signaling molecules as well as by controlling expression (Bedard and Krause, 2007; Lambeth et al., 2007; Brown and Griendling, 2009; Brandes et al., 2014). Thus, a comprehensive knowledge of NOX isoform expression could inform future studies on the regulation and function of different NOX isoforms.

NOX2 is the first isoform to be identified and characterized. It is expressed in phagocytes, which use NOX2-derived ROS for bacterial killing (Nauseef, 2004). Following the initial discovery of NOX2, several additional isoforms were identified in multicellular organisms, including NOX1, NOX3, NOX4, NOX5, DUOX1, and DUOX2 in humans (Fig. 1A) (Kawahara et al., 2007). In the human cardiovascular system, NOX1, NOX2, NOX4,

Grant sponsor: National Science Foundation; Grant number: 1146944-IOS; Grant sponsor: Purdue Research Foundation.

*CORRESPONDENCE TO: Daniel Suter, Department of Biological Sciences, Purdue University, 915 West State Street, West Lafayette, IN 47907-2054. E-mail: dsuter@purdue.edu

Received July 13, 2015; Revised November 3, 2015;
Accepted November 24, 2015.
DOI 10.1002/cne.23938
Published online December 29, 2015 in Wiley Online Library (wileyonlinelibrary.com)

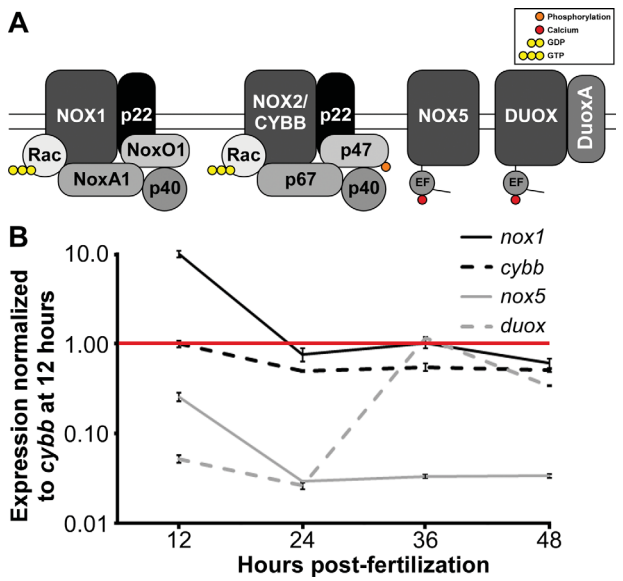

Figure 1. nox genes are expressed during early zebrafish development. **A**: Schematic of subunit composition of zebrafish NADPH oxidase complexes. NOX1, NOX2/CYBB, NOX5, and DUOX complexes are shown in their "active" state. NOX1 and NOX2/CYBB are activated by cytosolic subunits, whereas NOX5 and DUOX are activated by calcium. **B**: Relative expression levels derived via quantitative PCR from each of the four zebrafish NOX genes normalized to *cybb* at 12 hpf. *cybb* was chosen to normalize the dataset, as it was the most consistently expressed isoform. $n = 6$ for each data point. Error bars = SEM from all six data points.

and NOX5 are expressed in vascular smooth muscle cells (Jay et al., 2008; Zimmerman et al., 2011; Xu et al., 2014) as well as in endothelial cells (BelAiba et al., 2007; Drummond and Sobey, 2014). NOX activity is involved in blood pressure regulation and can lead to hypertension if out of control (Bedard and Krause, 2007). In the reproductive systems, NOX1 and NOX5 have been detected in human uterine tissue (Cheng et al., 2001; Brown and Griendling, 2009), whereas testis and ovary express NOX2, NOX4, and NOX5 (Cheng et al., 2001; Banfi et al., 2004b). NOX isoforms are also found in several other tissues including rabbit fibroblasts (NOX2), fish keratinocytes (DUOX), human kidneys (NOX1/2/4/5), human epithelial tissues of the colon (NOX1) and lung (DUOX), and human thyroid tissue (DUOX) (Pagano et al., 1997; De Deken et al., 2000; Harper et al., 2006; Bedard and Krause, 2007; Rokutan et al., 2008; Rieger and Sagasti, 2011; Holterman et al., 2015; Zhu et al., 2015).

Of particular interest to the present study is the expression of NOX in the nervous system. NOX1, NOX2, and NOX4 have been identified in cultured neurons derived from both the peripheral and the central nervous system (Hilburger et al., 2005; Tejada-Simon et al., 2005; Coyoy et al., 2008; Cao et al., 2009; Sorce and Krause, 2009; Choi et al., 2012; Kallenborn-Gerhardt et al., 2012; Munnamalai et al., 2014; Wilson et al., 2015). NOX3 is expressed in inner ear neurons (Banfi et al., 2004a) and has been implicated in balance based on swimming defects observed in NOX3 mutant mice (Paffenholz et al., 2004). Not surprisingly, NOX1 and NOX2 are also expressed in microglia, the phagocyte-like cells with immune function in the central nervous system (Wu et al., 2006; Cheret et al., 2008; Fischer et al., 2012). With respect to neuronal functions, NOX proteins have been implicated in neuronal stem cell maintenance in the brain (Dickinson et al., 2011), cerebellar development (Coyoy et al., 2013), neuronal differentiation (Tsatmali et al., 2006), neuronal polarity and neurite outgrowth (Munnamalai and Suter, 2009; Munnamalai et al., 2014; Olguin-Albuerne and Moran, 2015; Wilson et al., 2015), and synaptic plasticity (Kishida et al., 2006).

As detailed above, different NOX enzymes are found in many tissue types including in the nervous system and perform critical functions in these cells. In several cases, different NOX isoforms have been identified in the same tissue or even cell types; however, the functional relationship of the individual isoforms is often unclear. NADPH oxidase appears to have important roles in neuronal development; however, a systematic, tissue-scale characterization of NOX isoform expression throughout development of the nervous system has not been performed so far. In part, this is due to the limited availability of antibodies against several NOX isoforms in a number of species including zebrafish (*Danio rerio*)

Abbreviations

3V	third ventricle
CYBB	cytochrome B-245
DC	diencephalon
DIG	digoxigenin
DUOX	dual oxidase
E	eye
hpf	hour post-fertilization
ISH	in situ hybridization
MC	mesencephalon
MyC	myelencephalon
NC	notochord
NOX	nicotinamide dinucleotide phosphate oxidase
ON	optic nerve
OV	otic vesicle
PTU	N-phenylthiourea
qPCR	quantitative polymerase chain reaction
ROS	reactive oxygen species
SC	spinal cord
SM	somites
SSC	saline sodium citrate
TC	telencephalon
Tec	tectum
TecV	tectal ventricle

(Altenhofer et al., 2012). Furthermore, the current expression data from antibodies lacks validated support from other methods such as in situ hybridization (ISH) (Nayernia et al., 2014). Tissue-specific NOX expression has often been reported in the form of western blot data involving mixed cell populations. Some studies have shown cell-type–specific expression of NOX in cultured cells, but these are often limited to specific isoforms (Kishida et al., 2006; Munnamalai et al., 2014; Wilson et al., 2015) and therefore fail to show the contributions, if any, of other NOX isoforms in the same cell type. In addition, immunolocalization studies using cell cultures often focus on a specific cell type. Thus, only a few studies have investigated NOX isoform expression in a broad range of tissues during development and into adulthood (Cheng et al., 2001). These authors found that NOX5 is expressed in all human fetal tissues but later becomes restricted to specific adult tissue such as the uterus (Cheng et al., 2001). In summary, a comprehensive NOX isoform expression analysis in the developing nervous system is missing. Expression data would not only confirm/identify the neuronal source of ROS for established functions but potentially unveil new functions of ROS signaling in neurons.

Here, we analyzed expression of NOX isoforms during early zebrafish development. Zebrafish have been used to study several NOX functions including neutrophil migration, wound healing, and axon regeneration (Niethammer et al., 2009; Rieger and Sagasti, 2011; Yoo et al., 2011; Yan et al., 2014; de Oliveira et al., 2015). Sequences for *nox1, nox2* (also called cytochrome B-245 or *cybb*), *nox4, nox5*, and *duox* genes have been identified in the zebrafish genome. *nox4*, however, is not well annotated and consists of multiple transcripts; in addition, the suggested mRNA sequence does not align well with other known *nox4* gene sequences. Therefore, we decided to focus our expression analysis on the other four isoforms. Humans express two distinct isoforms of *duox* (1/2), whereas zebrafish express only a single isoform (Niethammer et al., 2009; Rigutto et al., 2009). To expand the current knowledge of NOX function in zebrafish nervous system development and regeneration, it is critical to know the spatiotemporal expression pattern of NOX genes. We used quantitative polymerase chain reaction (qPCR) along with ISH to characterize expression of *nox1, nox2/cybb, nox5*, and *duox* in the embryonic zebrafish during the first 48 hours after fertilization, which coincides with the development of major aspects of the zebrafish central nervous system (Schmidt et al., 2013). We identified dynamic changes in expression levels among three of the four isoforms studied. Furthermore, we found broad expression of all NOX isoforms during early development, which becomes more enhanced in specific regions of the brain at later developmental stages.

MATERIALS AND METHODS

Zebrafish housing/breeding

All animal work and experimental protocols were approved by the Purdue Animal Care and Use Committee. Zebrafish (*Danio rerio*) of the AB line (RRID:-ZIRC_ZL1) were maintained according to standard procedures (Westerfield, 2000; Hensley and Leung, 2010). Parental fish were set in pairs, and embryos were collected 15 minutes after breeding to obtain cohorts of the same stage. Embryos were maintained in E3 medium at 28 °C and staged as described prior to harvest (Kimmel et al., 1995). Between 12 and 23 hours post fertilization (hpf), 0.003% N-phenylthiourea (PTU) (Sigma, St. Louis, MO) in E3 medium was applied to embryos used for ISH to inhibit melanization (Li et al., 2012).

Quantitative PCR

Total RNA was isolated from 12, 24, 36, and 48 hpf embryos with TRIzol reagent (Life Technologies, Carlsbad, CA). The 36 and 48 hpf embryos were anesthetized with 0.016% tricaine methanesulfonate (Sigma) prior to RNA isolation. First-strand cDNA was prepared using the polyA primers supplied in the SuperScript®III First-Strand Synthesis System (Life Technologies). Primer sets against *nox1, nox2/cybb*, and *nox5*, and *duox, β-actin*, and *ribosomal protein L13a* were designed to target exons using ProbeFinder software (version 2.50, Roche Diagnostics, Indianapolis, IN) (see Table 1 for a summary of primer sequences). For each gene and each stage, samples were analyzed in three independent wells in a single 96-well plate. The experiment was repeated with two biological replicates of total RNA isolated from independent cohorts of embryos. Samples were run in a LightCycler96 (Roche Diagnostics,) for 35 cycles, and the relative expression levels were analyzed with the accompanying software (version 1.0.0.1240; RRID: rid_000088). Relative expression levels were calculated by using the cumulative ratio of the cycle threshold of the target gene to the cycle threshold of two reference genes (*rpl13a* and *β -actin*). These two genes were chosen as they show the most consistent expression pattern of commonly used reference genes (Tang et al., 2007). These calculated values were then normalized against the relative expression value for *nox2/cybb* at 12 hpf. *nox2/cybb* was chosen for normalization because of the stability of expression throughout the testing period. One-way analysis of variance (ANOVA) and direct comparisons via Dunnett's post

TABLE 1.
Primers Used for Quantitative Polymerase Chain Reaction (qPCR)

Gene	Gene ID	Primer	5′ to 3′
nox1	NM_001102387.1	NOX1_qPCR_forward	GCTCCAAGACTCCAGTGAATTA
nox1	NM_001102387.1	NOX1_qPCR_reverse	GACCCGCAATACTGGTGAATA
cybb	NM_200414.1	CYBB_qPCR_forward	CTTTCGTTATGAAGCGGTGATG
cybb	NM_200414.1	CYBB_qPCR_reverse	GGTTCTCCTGGACGTGTTTAT
nox5	XM_009297785.1	NOX5_qPCR_forward	TCATGTGCCGCTATCGTATG
nox5	XM_009297785.1	NOX5_qPCR_reverse	CCACCTTCCTCAGCTTCATT
duox	XM_001919359.5	DUOX_qPCR_forward	CCTGGGAGGACTTTCACTTTC
duox	XM_001919359.5	DUOX_qPCR_reverse	CTTGTGCTGTCTGCCTAGTT
rpl13a	NM_212784.1	Rpl13a_qPCR_forward	TCCTCCGCAAGAGAATGAAC
rpl13a	NM_212784.1	Rpl13a_qPCR_reverse	TGTGTGGAAGCATACCTCTTAC
β-actin	NM_007393.3	Bactin_qPCR_forward	CCTTCCAGCAGATGTGGATTAG
β-actin	NM_007393.3	Bactin_qPCR_reverse	TGAAGTGGTAACAGTCCGTTTAG

hoc analyses were carried out using GraphPad Prism software version 6.05 (RRID: rid_000081).

In situ hybridization

Probe sequences were amplified from 3-day-old zebrafish cDNA, prepared as described above, and cloned into the pGEM-T Easy vector (Promega, Madison, WI). The primers used for amplification are indicated in Table 2. Probe sequences were selected by aligning the zebrafish NOX genes, and identifying isoform-specific regions. Each prospective sequence was then used as the query for a BLAST search against the zebrafish RefSeq RNA database. The selected probes did not align to any other gene besides the target. The sizes of the riboprobes are as follows: *nox1*, 207 nucleotides (NM_001102387.1 position 645–851); *nox2/cybb*, 207 nucleotides (NM_200414.1 position 719–925); *nox5*-202 nucleotides (XM_009297785.1 position 512–713); and *duox*, 1,000 nucleotides (XM_001919359.5 position 1013–2012). Probe-containing vectors were then linearized, and riboprobes were synthesized using the DIG RNA Labeling Kit (Roche Diagnostics) and purified with 4M LiCl (Sigma) precipitation.

The ISH protocol was adapted from previous reports (Thisse and Thisse, 2008; Hensley et al., 2011). Whole-embryos were anesthetized in 0.016% tricaine methanesulfonate (Sigma) at 24, 36, and 48 hpf before fixation in 4% paraformaldehyde in phosphate-buffered saline (PBS; Sigma). Samples from the same time-point were processed together. The samples were then dehydrated stepwise in methanol (30%, 50% 70%, 100%), digested with 10 μg/mL Proteinase K (Worthington Biochemical, Lakewood, NJ) for 5 minutes (24 hpf), 12 minutes (36 hpf), or 20 minutes (48 hpf), and prehybridized in hybridization buffer (50% formamide, 5 × saline sodium citrate [SSC], 0.1% Tween 20, 5 mg/mL torula RNA, 50 μg/mL heparin) overnight at 65 °C. Embryos were then incubated overnight with 100 ng of riboprobe in 0.5 mL of hybridization buffer at 65 °C. Excess and imperfectly bound probes were then removed by washing twice with 50% formamide/2 × SSCT (SSC, 0.1% Tween 20) at 65 °C, once in 2 × SSCT, and twice in 0.2 × SSCT. Finally, embryos were washed twice with PBST (1 × PBS, 0.1% Tween 20). Anti-digoxigenin (DIG) antibodies (Roche Diagnostics) were preadsorbed by diluting 1:1,000 in blocking solution (2 mg/mL bovine serum albumin, 2% normal sheep serum, 1 × PBST) containing ≥ 50 embryos of various stages overnight at 4 °C on a shaker. RNA-hybridized embryos were incubated in blocking solution for 2 hours at room temperature. DIG-containing riboprobes were labeled overnight at 4 °C on a rocker with preadsorbed anti-DIG antibody diluted 1:3 in blocking solution. Excess antibody was removed with five washes in PBST and three washes in

TABLE 2.
Primers Used for In Situ Hybridization (ISH)

Gene	Gene ID	Primer	5′ to 3′
nox1	NM_001102387.1	NOX1_ISH_forward	TGCTGGTTTAGTTTTCCACG
nox1	NM_001102387.1	NOX1_ISH_reverse	AGCAGCCGTTCACAAATGTA
cybb	NM_200414.1	CYBB_ISH_forward	CATTGGATTGGTGCTTCATG
cybb	NM_200414.1	CYBB_ISH_reverse	CTCTCACAGACATACAGGAACATG
nox5	XM_009297785.1	NOX5_ISH_forward	ACAACAGTGGCTCCATCACA
nox5	XM_009297785.1	NOX5_ISH_reverse	CCGTACAGGCAAAGGAAGAAG
duox	XM_001919359.5	DUOX_ISH_forward	ATATAAAAGGAACAGGACGTGTCA
duox	XM_001919359.5	DUOX_ISH_reverse	GAAGGTCTGGAAAACTTTCTTCTC

staining buffer (100 mM Tris, pH 9.5, 50 mM $MgCl_2$, 100 mM NaCl, 0.1% Tween 20, 1 mM levamisol). The colorimetric reaction was carried out by incubation in nitroblue tetrazolium/5-bromo-4-chloro-3-indolyl-phosphate (Sigma) diluted in water at room temperature until slight color was visible in the sense control samples. The incubation times were kept consistent among time points for each gene (*nox1* for 3 hours, *cybb* for 3 hours, *nox5* for 4 hours, and *duox* for 2.5 hours). Nonspecific signals were washed out with a series of methanol washes (30%, 50% 70%, 100%) and a 1-minute incubation in benzyl alcohol/benzyl benzoate solution (2:1). Finally, the destained embryos were rehydrated with a series of methanol washes (100%, 70% 50%, 30%) and three washes in PBST.

Labeled embryos were stored in 4% paraformaldehyde in PBS at 4 °C and imaged as whole-mounts on a microscope slide in 3% methylcellulose using an Olympus SZX16 stereo microscope (Olympus, Center Valley, PA) with an SDF PLAPO 1×PF objective prior to being embedded in blocks of Tissue Freezing Media (Triangle Biosciences, Cincinnati, OH). A series of 10-μm transverse sections was collected from the most anterior region of the embryo through the spinal cord using a Leica CM 1510S cryostat (Leica Biosystems, Buffalo Grove, IL). Sections were mounted on microscope slides in VectaMount permanent mounting medium (Vector, Burlingame, CA). Cryosections were imaged on an Olympus BX51 upright microscope at with UPlanFL 10×/0.3 and UPlanS Apo 20×/0.75 objectives, respectively (Olympus). Images from both microscopes were captured by using a SPOT RT3 2.0Mp Slider CCD camera (SPOT Imaging Solutions, Sterling Heights, MI). At minimum, five individual samples were processed for each gene and time-point combination.

RESULTS

nox1

In the present study, we investigated the expression of *nox1, cybb, nox5*, and *duox* genes at the mRNA level during the first 48 hours after fertilization in developing zebrafish embryos. The molecular compositions of the respective NADPH oxidase complexes for each of these isoforms are shown in Figure 1A. qPCR performed on mRNA extracted from whole zebrafish embryos showed that *nox1* expression was the highest, at 12 hpf, among all four isoforms investigated (Fig. 1B). After this time point, the *nox1* expression decreased nearly 10-fold and remained consistent at this level throughout the next 36 hours ($P < 0.0001$ at 12 hpf versus 24, 36, and 48 hpf). We next used ISH with single-stranded, antisense RNA probes to investigate *nox1* gene expression in the nervous system of developing zebrafish embryos at 24, 36, and 48 hpf (Fig. 2). We did not use 12 hpf embryos for ISH because our main focus was on the nervous system, and no significant nervous system development has occurred at this stage. Images of whole-mount embryos demonstrated that *nox1* expression was broad in the head and anterior spinal cord (Fig. 2A–C). Next, we made 10-μm-thick transverse tissue sections from in situ hybridized embryos to provide a higher spatial resolution profile of *nox1* expression in the forebrain (Fig. 2E–H), eye (Fig. 2I–L), midbrain (Fig. 2M–P), hindbrain (Fig. 2Q–T), and anterior spinal cord (Fig. 2U–X). At 24 and 36 hpf, *nox1* expression was relatively uniform in all of these regions. By 48 hpf, *nox1* expression was slightly elevated in the region corresponding to the optic tectum (Fig. 2O) and the dorsal region of the spinal cord (Fig. 2W).

nox2/cybb

Nomenclature for NOX2 varies among species. In zebrafish, it is commonly referred to as cytochrome b-245 beta polypeptide (*cybb*; GenBank ID 393386). As assessed via qPCR, *cybb* expression levels display marked consistency during the first 2 days of development in comparison with the other NOX isoforms (Fig. 1B). Images of whole-mount ISH embryos showed broad expression of *cybb* throughout the head and spinal cord (Fig. 3A–D). Similarly to *nox1, cybb* was broadly expressed in all tissues examined during the first 36 hours (Fig. 3E,F, I,J, M,N, Q,R, U,V). By 48 hpf, the region of the midbrain corresponding to the optic tectum showed a slight increase in *cybb* expression (Fig. 3O). *cybb* remained broadly expressed in the forebrain, eye, hindbrain, and spinal cord.

nox5

qPCR results indicated that *nox5* had a similar expression profile as *nox1* but at a significantly lower level (Fig. 1B). *nox5* reached peak expression at 12 hpf, but exhibited lower expression levels by 24 hpf, which remained constant until 48 hpf ($P < 0.0001$ at 12 hpf vs. 24, 36, and 48 hpf). By 36 hpf, *nox5* exhibited the lowest expression levels of any NOX isoform during zebrafish development. Both whole-mounts and transverse tissue sections of ISH embryos demonstrated that *nox5* was broadly expressed throughout the nervous system at 24 and 36 hpf, similarly to *nox1* and *nox2* (Fig. 4A,B, E,F, I,J, M,N, Q,R, U,V). By 48 hpf, *nox5* showed a small increase in expression levels dorsally along the anterior–posterior axis from the forebrain (Fig. 4G) to the spinal cord (Fig. 4W).

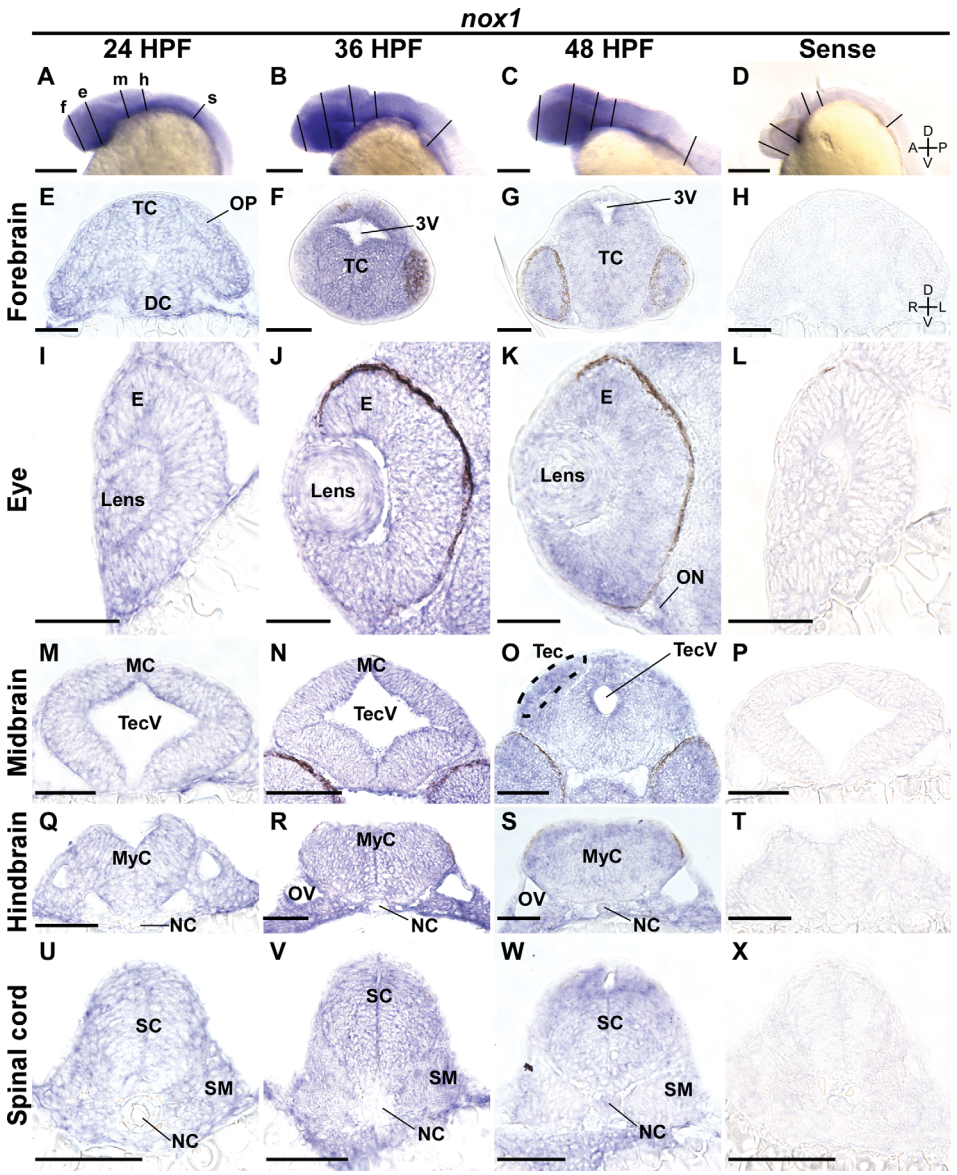

Figure 2. Broad nox1 expression through the first 2 days of development. **A–D**: Lateral views of whole-mount ISH embryos probed with antisense (**A–C**) and sense control (**D**) riboprobe against zebrafish *nox1* mRNA. Lines represent the position of sections shown in E-X. **E–H**: 10-μm-thick transverse sections through the forebrain (line labeled "f" in A) of 24, 36, and 48 hpf embryos incubated with antisense probes (**E–G**, respectively) and 24 hpf embryo incubated with a sense control probe (**H**). **I–L**: Transverse sections through the eye (line labeled "e" in A). **M–P**: Corresponding midbrain sections (line labeled "m" in A). **Q–T**: Corresponding hindbrain sections (line labeled "h" in A). **U–X**: Corresponding spinal sections (line labeled "s" in A). Abbreviations: 3V, third ventricle; DC, diencephalon; E, eye; MC, mesencephalon; MyC, myelencephalon; NC, notochord; ON, optic nerve; OV, otic vesicle; SC, spinal cord; SM, somites; TC, telencephalon; Tec, tectum; TecV, tectal ventricle. Scale bar = 0.5 mm in A–D; 100 μm in E–X.

duox

At 12 hpf, total *duox* expression was lower than any other NOX isoform. *duox* remained at this low level until 36 hpf, when expression increased by more than 10-fold ($P = 0.0001$ at 36 hpf vs. 12 and 24 hpf). High expression levels similar to *cybb* and *nox1* were maintained from 36 hpf to 48 hpf (Fig. 1B). *duox* was the only NOX isoform to undergo such a significant increase in expression during the first 48 hours of development. Similarly to the other three NOX isoforms, whole-mount ISH embryos and tissue sections through the head and spinal cord at 24 and 36 hpf demonstrated that *duox* expression was relatively broad (Fig. 5A,B, E,F, I,J, M,N, Q,R, U,V). By 48 hpf, *duox* expression domains became more unique. In the midbrain of 48 hpf fish, *duox* demonstrated a unique expression pattern that clearly deviated from any other NOX isoforms. *duox* was highly expressed in small regions

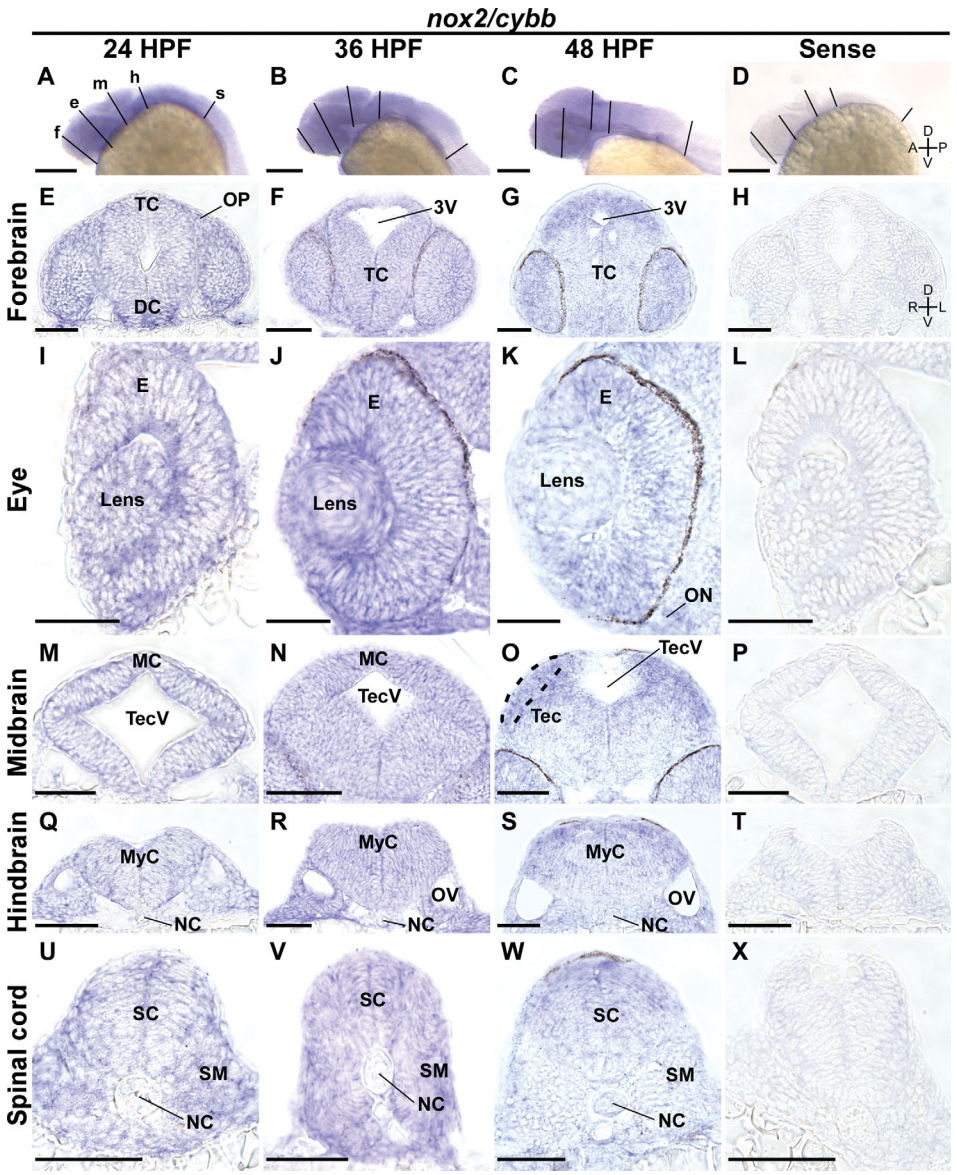

Figure 3. Broad nox2/cybb expression through the first two days of development. **A–D**: Lateral views of whole-mount ISH embryos probed with antisense (**A–C**) and sense control (**D**) riboprobe against zebrafish *nox2/cybb* mRNA. Lines represent the position of sections shown in E-X. **E–H**: 10-μm-thick transverse sections through the forebrain (line labeled "f" in A) of 24, 36, and 48 hpf embryos incubated with antisense probes (**E–G**, respectively) and 24 hpf embryo probed with a sense control (**H**). **I–L**: Transverse sections through the eye (line labeled "e" in A). **M–P**: Corresponding midbrain sections (line labeled "m" in A). **Q–T**: Corresponding hindbrain sections (line labeled "h" in A). **U–X**: Corresponding spinal sections (line labeled "s" in A). Abbreviations: 3V, third ventricle; DC, diencephalon; E, eye; MC, mesencephalon; MyC, myelencephalon; NC, notochord; ON, optic nerve; OV, otic vesicle; SC, spinal cord; SM, somites; TC, telencephalon; Tec, tectum; TecV, tectal ventricle. Scale bar = 0.5 mm in A–D; 100 μm in E–X.

surrounding the tectal ventricle, rather than broadly expressed in the dorsal region, as found for *nox5* (Fig. 5O). Furthermore, *duox* expression was not increased in the tectum, unlike the other three isoforms. In the spinal cord, *duox* was expressed throughout the neural tissue of 48 hpf fish, with a slight increase on the dorsal side (asterisk in Fig. 5W). In summary, similarly to the other NOX isoforms, *duox* exhibited a relatively broad expression pattern in the developing zebrafish nervous system until 48 hpf, when more distinct expression domains appeared.

DISCUSSION

NOX enzymes are a family of multi-subunit enzyme complexes, and each NOX isoform is subject to a unique type of regulation (Fig. 1A). This makes NOX enzymes excellent candidates to participate in cellular

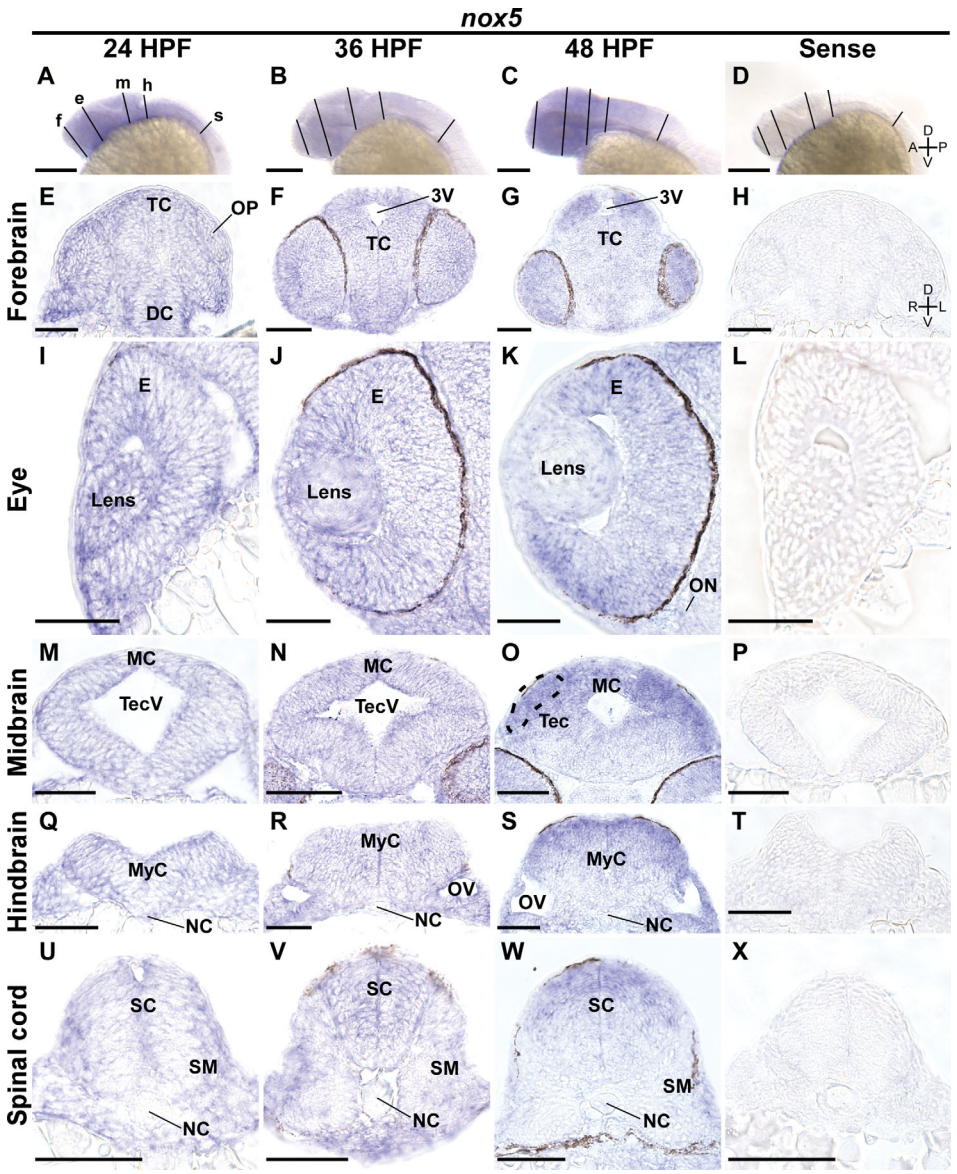

Figure 4. Broad nox5 expression through the first 2 days of development. **A–D**: Lateral views of whole-mount ISH embryos probed with antisense (**A–C**) and sense control (**D**) riboprobe against zebrafish *nox5* mRNA. Lines represent the position of sections shown in E–X. **E–H**: 10-μm-thick transverse sections through the forebrain (line labeled "f" in A) of 24, 36, and 48 hpf embryos incubated with antisense probes (**E–G**, respectively) and 24 hpf embryo probed with a sense control (**H**). **I–L**: Transverse sections through the eye (line labeled "e" in A). **M–P**: Corresponding midbrain sections (line labeled "m" in A). **Q–T**: Corresponding hindbrain sections (line labeled "h" in A). **U–X**:. Corresponding spinal sections (line labeled "s" in A). Abbreviations: 3V, third ventricle; DC, diencephalon; E, eye; MC, mesencephalon; MyC, myelencephalon; NC, notochord; ON, optic nerve; OV, otic vesicle; SC, spinal cord; SM, somites; TC, telencephalon; Tec, tectum; TecV, tectal ventricle. Scale bar = 0.5 mm in **A–D;** 100 μm in **E–X**.

signaling in response to specific upstream stimuli. Within the nervous system, NOX isoforms have been shown to function in astrocytes, microglia, and neurons (Sorce and Krause, 2009; Fischer et al., 2012; Nayernia et al., 2014). NOX hyperactivity plays a role in the development and progression of neurodegenerative diseases such as Alzheimer's, Parkinson's, and amyotrophic lateral sclerosis (Bedard and Krause, 2007). Despite these well-publicized deleterious roles, NOX enzymes also have important functions in normal central and peripheral nervous system development and function (Sorce and Krause, 2009; Nayernia et al., 2014). These include neuronal stem cell maintenance (Dickinson et al., 2011), cerebellar development (Coyoy et al., 2013; Olguin-Albuerne and Moran, 2015), neuronal differentiation (Tsatmali et al., 2006), neuronal polarity and neurite outgrowth (Munnamalai and Suter, 2009; Munnamalai et al., 2014; Wilson et al., 2015),

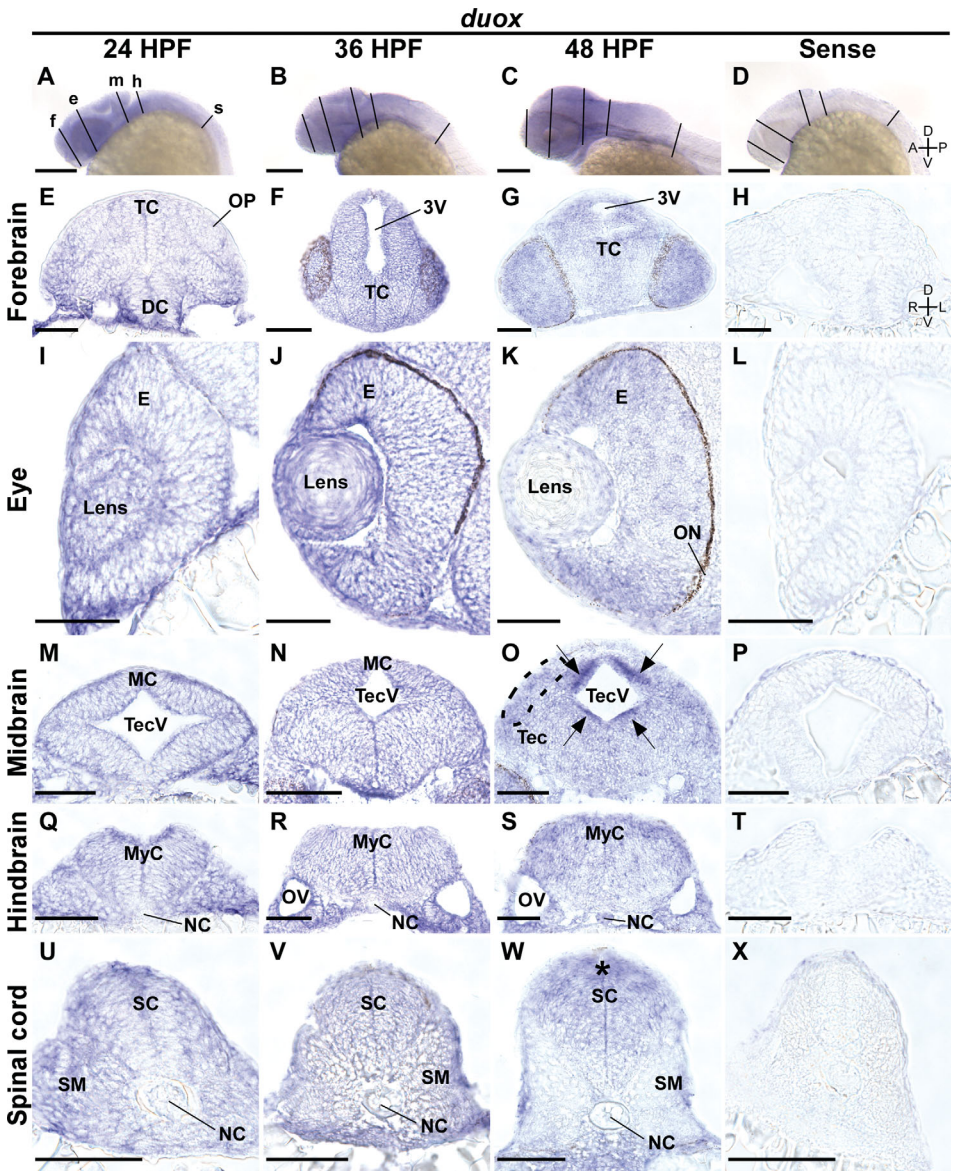

Figure 5. duox is highly expressed around tectal ventricle at 48 hpf . **A–D**: Lateral views of whole-mount ISH embryos probed with antisense (**A–C**) and sense control (**D**) riboprobe against zebrafish *duox* mRNA. Lines represent the position of sections shown in E–X. **E–H**: 10-μm-thick transverse sections through the forebrain (line labeled "f" in A) of 24, 36, and 48 hpf embryos incubated with antisense probes (**E–G**, respectively) and 24 hpf embryo probed with a sense control (**H**). **I–L**: Transverse sections through the eye (line labeled "e" in A). **M–P**: Corresponding midbrain sections (line labeled "m" in A). High *duox* expression was detected around the tectal ventricle (arrows in O). **Q–T**: Corresponding hindbrain sections (line labeled "h" in A). **U–X**: Corresponding spinal sections (line labeled "s" in A). Asterisk and arrows represent regions and small areas of increased *duox* expression in the spinal cord and midbrain, respectively. Abbreviations: 3V, third ventricle; DC, diencephalon; E, eye; MC, mesencephalon; MyC, myelencephalon; NC, notochord; ON, optic nerve; OV, otic vesicle; SC, spinal cord; SM, somites; TC, telencephalon; Tec, tectum; TecV, tectal ventricle. Scale bar = 0.5 mm in **A–D;** 100 μm in **E–X**.

and synaptic plasticity (Kishida et al., 2006). However, comprehensive analyses of NOX expression in the nervous system, such as the current study, are crucial to better understand the role these enzymes plays in development, disease, and regeneration.

In this study, we provide a detailed characterization of NOX expression within the nervous system of the developing zebrafish embryo. Sequences for *nox1, cybb, nox5*, and *duox* genes have been identified in the zebrafish genome; however, when and where individual NOX genes are expressed in fish embryos is currently unknown. We used qPCR (Fig. 1B) and ISH (Figs. 2–5) to characterize the expression of *nox1, cybb, nox5*, and *duox* in the developing fish nervous system between 12 and 48 hpf. qPCR data show dynamic changes in *nox1, nox5*, and *duox* expression, whereas *cybb* levels are

remarkably consistent from 12 to 48 hpf. Whole-mount ISH data are overall qualitatively in agreement with the qPCR data; however, it is important to keep in mind that ISH is not a quantitative method. Thus, proper quantification of ISH is difficult if not impossible between different time points and within tissues. All four NOX isoforms are broadly expressed in the early nervous system at 24 and 36 hpf. Whereas the broad expression continues, subtle differences in midbrain expression are visible by 48 hpf. *nox1, cybb*, and *nox5* show slightly elevated expression in the dorsal regions of the midbrain corresponding to the optic tectum. In contrast, *duox* expression was enriched in the regions adjacent to the tectal ventricle by this time. Increased labeling in dorsal and ventricle-adjacent regions was not observed in other samples using tissue of comparable thickness. Therefore we believe that the small increases in *nox1, cybb*, and *nox5* expression in the dorsal midbrain is real and not due to a technical artifact caused by incomplete probe penetration or probe trapping. Nonetheless, in most cases these increases are subtle and may not necessarily suggest functional significance.

One might wonder why the four zebrafish NOX isoforms show a very similar expression pattern early in development. A few points should be considered here. First, we have not assessed protein levels, because isoform-specific antibodies are still sparse and not well validated in the zebrafish model system. It is possible that different NOX isoforms show more distinct expression patterns at the protein level during first 2 days of zebrafish development depending on translational regulation. MicroRNAs have been shown to affect the activity of NOX4, the constitutively active isoform of NOX (Gordillo et al., 2014; Wang et al., 2014). Based on this information, it is plausible that other NOX isoforms could be post-transcriptionally regulated. Thus, it will be important to investigate the levels of protein expression in the developing nervous system. Second, broad NOX expression during early development is not without precedent, as NOX5 expression is present in all human fetal tissues but is more restricted in adult tissue (Cheng et al., 2001). Because of broad expression of all NOX isoforms early during development, knocking out one isoform might result in functional compensation by another NOX isoform, and therefore strong phenotypes would not be generated. This idea is supported by the fact that ROS levels in cultured cerebellar granule neurons derived from NOX2 knockout mice were not different from wild-type control neurons (Olguin-Albuerne and Moran, 2015). In addition, there is not much information in the literature about strong nervous system phenotypes of existing NOX knockout mouse models except for the mild impairments in hippocampus-dependent memory in NOX2 knockout mice (Kishida et al., 2006). Lastly, it is important to keep in mind that the different NOX isoforms have unique activation mechanisms, and the resulting ROS are expected to act locally close to the source. Thus, even if multiple isoforms are expressed in the same cell type at any given time, different upstream signals could activate distinct NOX isoforms, which act in specific functions such as cell differentiation, adhesion, or migration.

Our current data on broad expression of NOX genes suggest that NOX activity may be a central contributor during nervous system development. We are aware that the present expression data for the main enzymatic subunit of the NOX complex are not sufficient to form any conclusions about ROS levels in different regions of the nervous system. However, we believe that the results from this study will provide important information when interpreting the results of future studies addressing the function of NOX enzymes in embryonic zebrafish nervous system development and neurogenesis using pharmacological and molecular manipulations of activity and expression levels of NOX isoforms.

ACKNOWLEDGEMENTS

We thank Dr. Mark Quinn and Dr. Ahmad Athamneh for their constructive comments on this manuscript.

CONFLICT OF INTEREST STATEMENT

The authors declare no conflict of interest

ROLE OF AUTHORS

All authors had full access to all the data in the study and take responsibility for the integrity of the data and the accuracy of the data analysis. Study concept and design: DMS and CJW. Acquisition of data: CJW. Analysis and interpretation of data: CJW, YFL, and DMS. Drafting of the manuscript: CJW and DMS. Critical revision of the manuscript for important intellectual content: CJW, YFL, and DMS. Statistical analysis: CJW. Obtained funding: DMS and CJW. Study supervision: DMS.

LITERATURE CITED

Altenhofer S, Kleikers PW, Radermacher KA, Scheurer P, Rob Hermans JJ, Schiffers P, Ho H, Wingler K, Schmidt HH. 2012. The NOX toolbox: validating the role of NADPH oxidases in physiology and disease. Cell Mol Life Sci 69: 2327–2343.

Banfi B, Malgrange B, Knisz J, Steger K, Dubois-Dauphin M, Krause KH. 2004a. NOX3, a superoxide-generating NADPH oxidase of the inner ear. J Biol Chem 279: 46065–46072.

Banfi B, Tirone F, Durussel I, Knisz J, Moskwa P, Molnar GZ, Krause KH, Cox JA. 2004b. Mechanism of Ca2 + activation

of the NADPH oxidase 5 (NOX5). J Biol Chem 279:18583–18591.
Bedard K, Krause KH. 2007. The NOX family of ROS-generating NADPH oxidases: physiology and pathophysiology. Physiol Rev 87:245–313.
BelAiba RS, Djordjevic T, Petry A, Diemer K, Bonello S, Banfi B, Hess J, Pogrebniak A, Bickel C, Gorlach A. 2007. NOX5 variants are functionally active in endothelial cells. Free Radic Biol Med 42:446–459.
Brandes RP, Weissmann N, Schroder K. 2014. Nox family NADPH oxidases: molecular mechanisms of activation. Free Radic Biol Med 76:208–226.
Brown DI, Griendling KK. 2009. Nox proteins in signal transduction. Free Radic Biol Med 47:1239–1253.
Cao X, Demel SL, Quinn MT, Galligan JJ, Kreulen D. 2009. Localization of NADPH oxidase in sympathetic and sensory ganglion neurons and perivascular nerve fibers. Auton Neurosci 151:90–97.
Cheng G, Cao Z, Xu X, van Meir EG, Lambeth JD. 2001. Homologs of gp91phox: cloning and tissue expression of Nox3, Nox4, and Nox5. Gene 269:131–140.
Cheret C, Gervais A, Lelli A, Colin C, Amar L, Ravassard P, Mallet J, Cumano A, Krause KH, Mallat M. 2008. Neurotoxic activation of microglia is promoted by a nox1-dependent NADPH oxidase. J Neurosci 28:12039–12051.
Choi DH, Cristovao AC, Guhathakurta S, Lee J, Joh TH, Beal MF, Kim YS. 2012. NADPH oxidase 1-mediated oxidative stress leads to dopamine neuron death in Parkinson's disease. Antioxid Redox Signal 16:1033–1045.
Coyoy A, Valencia A, Guemez-Gamboa A, Moran J. 2008. Role of NADPH oxidase in the apoptotic death of cultured cerebellar granule neurons. Free Radic Biol Med 45:1056–1064.
Coyoy A, Olguin-Albuerne M, Martinez-Briseno P, Moran J. 2013. Role of reactive oxygen species and NADPH-oxidase in the development of rat cerebellum. Neurochem Int 62:998–1011.
De Deken X, Wang D, Many MC, Costagliola S, Libert F, Vassart G, Dumont JE, Miot F. 2000. Cloning of two human thyroid cDNAs encoding new members of the NADPH oxidase family. J Biol Chem 275:23227–23233.
de Oliveira S, Boudinot P, Calado A, Mulero V. 2015. Duox1-derived H2O2 modulates Cxcl8 expression and neutrophil recruitment via JNK/c-JUN/AP-1 signaling and chromatin modifications. J Immunol 194:1523–1533.
Dickinson BC, Peltier J, Stone D, Schaffer DV, Chang CJ. 2011. Nox2 redox signaling maintains essential cell populations in the brain. Nat Chem Biol 7:106–112.
Drummond GR, Sobey CG. 2014. Endothelial NADPH oxidases: which NOX to target in vascular disease? Trends Endocrinol Metab 25:452–463.
Finkel T. 2011. Signal transduction by reactive oxygen species. J Cell Biol 194:7–15.
Fischer MT, Sharma R, Lim JL, Haider L, Frischer JM, Drexhage J, Mahad D, Bradl M, van Horssen J, Lassmann H. 2012. NADPH oxidase expression in active multiple sclerosis lesions in relation to oxidative tissue damage and mitochondrial injury. Brain 135:886–899.
Forman HJ, Ursini F, Maiorino M. 2014. An overview of mechanisms of redox signaling. J Mol Cell Cardiol 73:2–9.
Gordillo GM, Biswas A, Khanna S, Pan X, Sinha M, Roy S, Sen CK. 2014. Dicer knockdown inhibits endothelial cell tumor growth via microRNA 21a-3p targeting of Nox-4. J Biol Chem 289:9027–9038.
Harper RW, Xu C, McManus M, Heidersbach A, Eiserich JP. 2006. Duox2 exhibits potent heme peroxidase activity in human respiratory tract epithelium. FEBS Lett 580: 5150–5154.
Hensley MR, Leung YF. 2010. A convenient dry feed for raising zebrafish larvae. Zebrafish 7:219–231.
Hensley MR, Emran F, Bonilla S, Zhang L, Zhong W, Grosu P, Dowling JE, Leung YF. 2011. Cellular expression of Smarca4 (Brg1)-regulated genes in zebrafish retinas. BMC Dev Biol 11:45.
Hilburger EW, Conte EJ, McGee DW, Tammariello SP. 2005. Localization of NADPH oxidase subunits in neonatal sympathetic neurons. Neurosci Lett 377:16–19.
Holterman CE, Thibodeau JF, Kennedy CR. 2015. NADPH oxidase 5 and renal disease. Curr Opin Nephrol Hypertens 24:81–87.
Jay DB, Papaharalambus CA, Seidel-Rogol B, Dikalova AE, Lassegue B, Griendling KK. 2008. Nox5 mediates PDGF-induced proliferation in human aortic smooth muscle cells. Free Radic Biol Med 45:329–335.
Kallenborn-Gerhardt W, Schroder K, Del Turco D, Lu R, Kynast K, Kosowski J, Niederberger E, Shah AM, Brandes RP, Geisslinger G, Schmidtko A. 2012. NADPH oxidase-4 maintains neuropathic pain after peripheral nerve injury. J Neurosci 32:10136–10145.
Kawahara T, Quinn MT, Lambeth JD. 2007. Molecular evolution of the reactive oxygen-generating NADPH oxidase (Nox/Duox) family of enzymes. BMC Evol Biol 7:109.
Kimmel CB, Ballard WW, Kimmel SR, Ullmann B, Schilling TF. 1995. Stages of embryonic development of the zebrafish. Dev Dyn 203:253–310.
Kishida KT, Hoeffer CA, Hu D, Pao M, Holland SM, Klann E. 2006. Synaptic plasticity deficits and mild memory impairments in mouse models of chronic granulomatous disease. Mol Cell Biol 26:5908–5920.
Lambeth JD, Kawahara T, Diebold B. 2007. Regulation of Nox and Duox enzymatic activity and expression. Free Radic Biol Med 43:319–331.
Li Z, Ptak D, Zhang L, Walls EK, Zhong W, Leung YF. 2012. Phenylthiourea specifically reduces zebrafish eye size. PloS One 7:e40132.
Montezano AC, Touyz RM. 2014. Reactive oxygen species, vascular Noxs, and hypertension: focus on translational and clinical research. Antioxid Redox Signal 20:164–182.
Munnamalai V, Suter DM. 2009. Reactive oxygen species regulate F-actin dynamics in neuronal growth cones and neurite outgrowth. J Neurochem 108:644–661.
Munnamalai V, Weaver CJ, Weisheit CE, Venkatraman P, Agim ZS, Quinn MT, Suter DM. 2014. Bidirectional interactions between NOX2-type NADPH oxidase and the F-actin cytoskeleton in neuronal growth cones. J Neurochem 130:526–540.
Nakanishi A, Wada Y, Kitagishi Y, Matsuda S. 2014. Link between PI3K/AKT/PTEN pathway and NOX proteinin diseases. Aging Dis 5:203–211.
Nauseef WM. 2004. Assembly of the phagocyte NADPH oxidase. Histochem Cell Biol 122:277–291.
Nayernia Z, Jaquet V, Krause KH. 2014. New insights on NOX enzymes in the central nervous system. Antioxid Redox Signal 20:2815–2837.
Niethammer P, Grabher C, Look AT, Mitchison TJ. 2009. A tissue-scale gradient of hydrogen peroxide mediates rapid wound detection in zebrafish. Nature 459:996–999.
Olguin-Albuerne M, Moran J. 2015. ROS produced by NOX2 control in vitro development of cerebellar granule neurons development. ASN Neuro 7(2).
Paffenholz R, Bergstrom RA, Pasutto F, Wabnitz P, Munroe RJ, Jagla W, Heinzmann U, Marquardt A, Bareiss A, Laufs J, Russ A, Stumm G, Schimenti JC, Bergstrom DE. 2004. Vestibular defects in head-tilt mice result from mutations in Nox3, encoding an NADPH oxidase. Genes Dev 18: 486–491.

Pagano PJ, Clark JK, Cifuentes-Pagano ME, Clark SM, Callis GM, Quinn MT. 1997. Localization of a constitutively active, phagocyte-like NADPH oxidase in rabbit aortic adventitia: enhancement by angiotensin II. Proc Natl Acad Sci U S A 94:14483–14488.

Rieger S, Sagasti A. 2011. Hydrogen peroxide promotes injury-induced peripheral sensory axon regeneration in the zebrafish skin. PLoS Biol 9:e1000621.

Rigutto S, Hoste C, Grasberger H, Milenkovic M, Communi D, Dumont JE, Corvilain B, Miot F, De Deken X. 2009. Activation of dual oxidases Duox1 and Duox2: differential regulation mediated by camp-dependent protein kinase and protein kinase C-dependent phosphorylation. J Biol Chem 284:6725–6734.

Rokutan K, Kawahara T, Kuwano Y, Tominaga K, Nishida K, Teshima-Kondo S. 2008. Nox enzymes and oxidative stress in the immunopathology of the gastrointestinal tract. Semin Immunopathol 30:315–327.

Schmidt R, Strahle U, Scholpp S. 2013. Neurogenesis in zebrafish–from embryo to adult. Neural Dev 8:3.

Sorce S, Krause KH. 2009. NOX enzymes in the central nervous system: from signaling to disease. Antioxid Redox Signal 11:2481–2504.

Tang R, Dodd A, Lai D, McNabb WC, Love DR. 2007. Validation of zebrafish (*Danio rerio*) reference genes for quantitative real-time RT-PCR normalization. Acta Biochim Biophys Sinica 39:384–390.

Tejada-Simon MV, Serrano F, Villasana LE, Kanterewicz BI, Wu GY, Quinn MT, Klann E. 2005. Synaptic localization of a functional NADPH oxidase in the mouse hippocampus. Mol Cell Neurosci 29:97–106.

Thisse C, Thisse B. 2008. High-resolution in situ hybridization to whole-mount zebrafish embryos. Nat Protoc 3:59–69.

Tsatmali M, Walcott EC, Makarenkova H, Crossin KL. 2006. Reactive oxygen species modulate the differentiation of neurons in clonal cortical cultures. Mol Cell Neurosci 33: 345–357.

Wang HJ, Huang YL, Shih YY, Wu HY, Peng CT, Lo WY. 2014. MicroRNA-146a decreases high glucose/thrombin-induced endothelial inflammation by inhibiting NAPDH oxidase 4 expression. Mediat Inflamm 2014:379537.

Westerfield M. 2000. The zebrafish book. A guide for the laboratory use of zebrafish (*Danio rerio*). Eugene, OR: University of Oregon Press.

Wilson C, Nunez MT, Gonzalez-Billault C. 2015. Contribution of NADPH oxidase to the establishment of hippocampal neuronal polarity in culture. J Cell Sci 128:2989–2995.

Wu DC, Re DB, Nagai M, Ischiropoulos H, Przedborski S. 2006. The inflammatory NADPH oxidase enzyme modulates motor neuron degeneration in amyotrophic lateral sclerosis mice. Proc Natl Acad Sci U S A 103:12132–12137.

Xu S, Chamseddine AH, Carrell S, Miller FJ, Jr. 2014. Nox4 NADPH oxidase contributes to smooth muscle cell phenotypes associated with unstable atherosclerotic plaques. Redox Biol 2:642–650.

Yan B, Han P, Pan L, Lu W, Xiong J, Zhang M, Zhang W, Li L, Wen Z. 2014. IL-1beta and reactive oxygen species differentially regulate neutrophil directional migration and basal random motility in a zebrafish injury-induced inflammation model. J Immunol 192:5998–6008.

Yoo SK, Starnes TW, Deng Q, Huttenlocher A. 2011. Lyn is a redox sensor that mediates leukocyte wound attraction in vivo. Nature 480:109–112.

Zhu K, Kakehi T, Matsumoto M, Iwata K, Ibi M, Ohshima Y, Zhang J, Liu J, Wen X, Taye A, Fan C, Katsuyama M, Sharma K, Yabe-Nishimura C. 2015. NADPH oxidase NOX1 is involved in activation of protein kinase C and premature senescence in early-stage diabetic kidney. Free Radic Biol Med 83:21–30.

Zimmerman MC, Takapoo M, Jagadeesha DK, Stanic B, Banfi B, Bhalla RC, Miller FJ Jr. 2011. Activation of NADPH oxidase 1 increases intracellular calcium and migration of smooth muscle cells. Hypertension 58:446–453.